Supramolecular Chemistry
Publication details, including instructions for authors and subscription information:
http://www.informaworld.com/smpp/title~content=t713649759

Free Energy Peturbation and Molecular Dynamics Simulation Studies on the Enantiomeric Discrimination of Amines by Dimethyldiketopyridino-18-Crown-6

One-Sun Lee[a]; Sungu Hwang[a]; Doo Soo Chung[a]
[a] Department of Chemistry, Seoul National University, Seoul, Korea

To cite this Article Lee, One-Sun , Hwang, Sungu and Chung, Doo Soo(2000) 'Free Energy Peturbation and Molecular Dynamics Simulation Studies on the Enantiomeric Discrimination of Amines by Dimethyldiketopyridino-18-Crown-6', Supramolecular Chemistry, 12: 3, 255 — 272
To link to this Article: DOI: 10.1080/10610270008029448
URL: http://dx.doi.org/10.1080/10610270008029448

SUPRAMOLECULAR CHEMISTRY, Vol. 12, pp. 255-272
Reprints available directly from the publisher
Photocopying permitted by license only

Free Energy Perturbation and Molecular Dynamics Simulation Studies on the Enantiomeric Discrimination of Amines by Dimethyldiketopyridino-18-Crown-6

ONE-SUN LEE, SUNGU HWANG and DOO SOO CHUNG*

Department of Chemistry, Seoul National University, Seoul 151–742, Korea

(Received July 26, 1999; Revised October 20, 1999)

Discrimination of chiral amines by dimethyldiketopyridino-18-crown-6 (**1**) is studied by free energy perturbation (FEP) and molecular dynamics (MD) methods. **1** has two (*S*)-chiral centers and discriminates chiral amines through host-guest interactions. The optically active amines in this study are α-(1-naphthyl)ethylamine, methylbenzylamine, cyclohexylethylamine, and *sec*-butylamine. The trends in binding free energy differences obtained from FEP calculations were in excellent agreement with experimental results obtained in the gas phase. In order to explain the enantioselectivity of the host in terms of the host-guest interactions at the molecular level, we analyzed the structures generated by 10-ns MD simulations of host-guest complexes. The suggested chiral discrimination mechanism, the π-π interaction and the steric repulsion between the guest and the host, was verified by our MD simulation analysis.

Keywords: Free Energy Perturbation (FEP), Molecular Dynamics (MD), pyridino-18-crown-6, chiral separation, gas phase

I. INTRODUCTION

The differing reactivities of enantiomers toward asymmetric compounds are strongly manifested in biological systems.[1] Often one enantiomer of a pharmaceutical, herbicide, or pesticide is responsible for the desired activity, while its mirror image is inactive or even exhibits side effects.[2] Thus chiral discrimination has been a longstanding problem in various fields. One of the most successful protocols for the resolution of enantiomers is based on host-guest chemistry. During the last few decades, extensive experimental studies on various chiral hosts including cyclodextrin,[3] bile salts,[4] and crown ethers[5,6] have been carried out. In particular, crown ethers have elicited much interest because of their potential importance in elucidating the mechanism responsible for enzyme action and membrane transport processes.[7] They bind guests such as alkali metal ions and protonated amines selectively,[8,9] and serve as simple models for selective host-guest binding[10]. It has been determined by various experimental methods that chirally substituted crown ethers differentiate amine enantiomers very successfully.[11,12] However, nearly all of these studies have been carried out in condensed media, and thus the results are subject to influences exerted by solvent and

* To whom correspondence should be addressed. Doo Soo Chung (e-mail) dschung@snu.ac.kr (Phone) +82-2-880-8130 (FAX) +82-2-877-3025

counterion molecules. In many cases, these complicating effects can obscure the fundamental components underlying and controlling the enantioselection.

Recently, Dearden et al. reported enantiomeric discrimination of dimethyldiketopyridino-18-crown-6 (**1**) toward various protonated amines by using Fourier transform ion cyclotron resonance (FTICR) mass spectrometry in the gas phase[13]. The gas phase experiments and theoretical investigations in vacuo can provide insights to probe the fundamentals of enantiomeric recognition, since they are not affected by solvent or counterion molecules. In the **1**-chiral amine complex system, π-π and steric interactions are suggested to be responsible for enantiomeric discrimination.[14,15] However, only a handful of theoretical investigations have been reported on this subject. Bradshaw et al. calculated the binding energy difference between **1** and (*R*)-α-(1-naphthyl)ethylamine complex and **1** and (*S*)-α-(1-naphthyl)ethylamine complex by an empirical forcefield technique.[16] The calculated binding energy difference was about 2.9 kJ/mol and was comparable with experimental results. However, they ignored the entropic contribution and thus the reported energy was enthalpic energy rather than free energy.

In this study, we employed free energy perturbation[17] (FEP) and molecular dynamics[18] (MD) simulations to explain the results of recent experiments on the enantioselectivity of the host (**1**) toward chiral guests: α-(1-naphthyl)ethylamine (**2**), methylbenzylamine (**3**), cyclohexylethylamine (**4**), and *sec*-butyl amine (**5**) (Figure 1) in vacuo. **1** has two (*S*)-chiral centers and discriminates chiral amines through host-guest interactions. The host-guest complexes are formed by three hydrogen bonds.[19] It was speculated that the chiral discrimination occurred by π-π and steric interactions between **1** and the protonated amine guest. Even though this idea was supported by a number of experiments,[14,16,20] it is important to carry out theoretical investigations to verify these suggested mechanisms. Theoretical methods that reproduce the experimental findings can be systematically applied to a series of hosts, and can help us to understand the features essential for the desired function of the host.[21] We were able with our theoretical results to reproduce the observed trends in selectivity as well as the structural issues. The deeper understanding of the enantioselectivity mechanism of crown ethers obtained in this study will be of great assistance not only for the rational design of potent chiral selectors but also in developing enantiomeric separation methods such as liquid chromatography and capillary electrophoresis.[11,22,23]

II. COMPUTATIONAL DETAILS

Choice of Starting Geometry

X-ray data available from the literature were used as the starting geometry for the (*S,S*)-**1** and (*R*, or *S*)-**2** complex structure.[19] Similarly, the starting geometry of the complex structure between (*S,S*)-**1** and (*R*, or *S*)-**3** was obtained by modification of the *X*-ray structure between (*S,S*)-**1** and $PhCH(CH_2OH)NH_3^+$.[20] Since the *X*-ray data of all other host-guest complex structure sets have not been reported so far, these structures were obtained from modification of the above data. All simulations were done with the AMBER* forcefield implemented in the MacroModel 5.5 package.[24] To obtain the minimum energy structure, MD and molecular mechanics calculations were carried out. The Monte Carlo/Stochastic Dynamics[25] (MC/SD) algorithm was adapted for the dynamics simulations. MD simulations were performed at 800 K for 2 ns with a 1-fs time step. Samples during the dynamics simulation were obtained every 100 fs, and then an energy minimization with a conjugate gradient algorithm was performed on every sampled structure to a gradient norm of less than 0.001 kJ/mol Å. All of the minimum energy

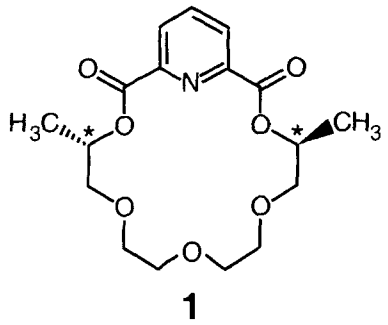

1

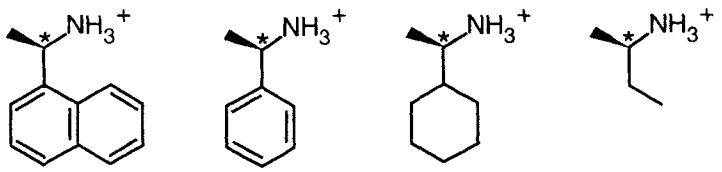

2 3 4 5

FIGURE 1 Structures of chiral host (**1**) and chiral protonated amine guests (**2–5**)

structures obtained by this procedure were used in the calculations including FEP and MD.

FEP Calculation

In order to compute the difference in binding energies between the two enantiomers of **2–5** with (*S,S*)-**1**, the thermodynamic cycle described in Scheme 1 was used. In this cycle, (*S,S* or *R,R*)-**1**:(*R* or *S*)-Guest denotes the complex structure of **1** and one of the enantiomeric guests. Since the Helmholtz free energy is a state function, the difference in binding Helmholtz free energies, $\Delta A_4 - \Delta A_3$, is the same as $\Delta A_2 - \Delta A_1$, i.e.,

$$\Delta\Delta A \equiv \Delta A_4 - \Delta A_3 = \Delta A_2 - \Delta A_1. \quad (1)$$

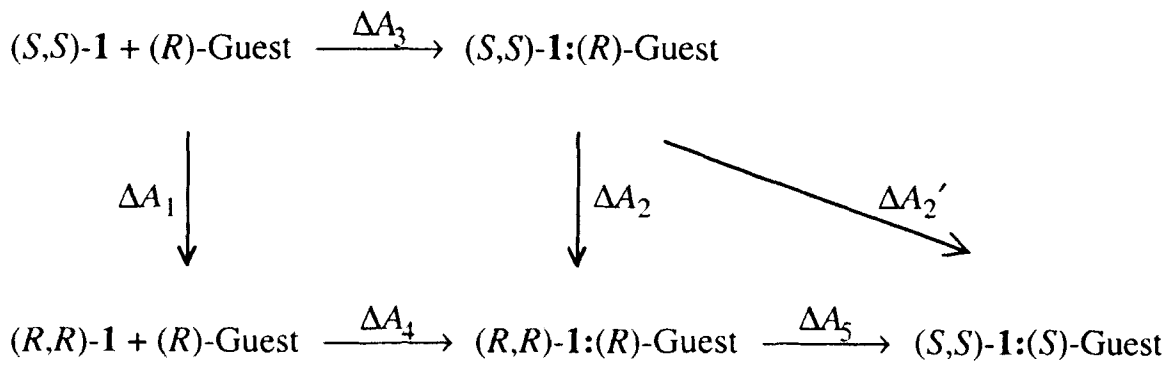

SCHEME 1

Usually the binding free energies ΔA_3 and ΔA_4 are measured by experiment, while ΔA_1 and ΔA_2 could be calculated by FEP simulations with relative ease. Since (*S,S*)-**1** and (*R,R*)-**1** have the same energy, ΔA_1 is zero. Thus only the ΔA_2 term is needed where the enantioselectivity is concerned. Even though the experiments were performed between (*S,S*)-**1**:(*R*)-Guest and (*R,R*)-**1**:(*R*)-Guest complexes (ΔA_2),[13] our theoretical investigations were performed between (*S,S*)-**1**:(*R*)-Guest and (*S,S*)-**1**:(*S*)-Guest complexes ($\Delta A_2'$) since (*R,R*)-**1**:(*R*)-Guest and (*S,S*)-**1**:(*S*)-Guest have the same energy due to the symmetry ($\Delta A_5 = 0$):

$$\Delta A_2 = \Delta A_2' - \Delta A_5 = \Delta A_2'. \quad (2)$$

We used the following standard FEP formula[17,26,27] for the calculation of $\Delta A_2'$:

$$\Delta A_2' = -k_B T \ln\langle \exp[-V_S - V_R)/k_B T]\rangle_S, \quad (3)$$

where $k_B T$ is the Boltzmann constant times the absolute temperature, and V_R and V_S are the potential energy functions of **1**:(*R*)-Guest and **1**:(*S*)-Guest complexes, respectively. Since all the configurations of host **1** in this paper are (*S,S*)-**1**, hereafter the notation **1** will be used for (*S,S*)-**1** for clarity. The symbol $< >_S$ refers to an ensemble average over a reference state represented by V_S. The perturbation we used mutates the (*S*)-Guest into the (*R*)-Guest by interchanging guest molecule residues (i.e., $CH_3 \rightarrow HDu_3$ and $HDu_3 \rightarrow CH_3$, where Du is a dummy atom) over 40 stages with double-wide sampling at each stage. A time step of 1 fs, an equilibration period of 100 ps, and a temperature of 300 K were used. 500 ps of sampling time was applied to all calculations. Since the configuration sampling was performed in a canonical ensemble at 300 K, the calculated free energy corresponds to the Helmholtz free energy. Although the difference between the Helmholtz free energy and the Gibbs free energy, $P\Delta V$ (= $(\Delta n)RT$, where P is pressure, V volume, n number of moles, R the gas constant, and T temperature), is not negligible, the relative difference between them ($P\Delta\Delta V$) is negligible, even in the gas phase.

FEP simulation has been proved to be a useful tool in studying various host-guest systems.[28,29] It allows calculation of free energy differences that can be directly compared with experimental results. Since FEP simulation calculates the energy *difference* between the two states (see Eq. 3), the error in the free energy difference is smaller than that from other methods which calculate the free energies of the two states *separately* and then obtain the difference by subtracting one from the other.[30]

Dynamics Analysis

Another computational method can be used to obtain the free energy difference.[31] The free energy difference $\Delta A_2'$ can be written as

$$\Delta A_2' = -k_B T \ln \frac{Z_S}{Z_R}, \quad (4)$$

where Z_S/Z_R is the ratio of the canonical partition functions for the states *S* and *R*, and is given by

$$\frac{Z_S}{Z_R} = \frac{\sum_i \exp(-E_{Si}/k_B T)}{\sum_n \exp(-E_{Rn}/k_B T)}. \quad (5)$$

The energies E_{Si} and E_{Rn} can be obtained from an adequate sampling of the phase space during the molecular dynamics and subsequent minimization of each structure. MD simulations of complex molecular systems have been shown to give not only the relative free energies of chemical states, but also important structural information. However, this is valid only when the phase space is covered adequately. We used the MC/SD algorithm, which generates a canonical ensemble and samples the phase space of the system more effectively than do stochastic dynamics or Monte Carlo simulation alone.[25] Of course, the total energies are much greater in magnitude and thus it is anticipated that the free energy difference in this simulation may suffer from larger uncertainties than that from the FEP calculation for a given period of computation time. However, MD at the two end points (which correspond to $\lambda = 0$ and $\lambda = 1$ in FEP) is useful

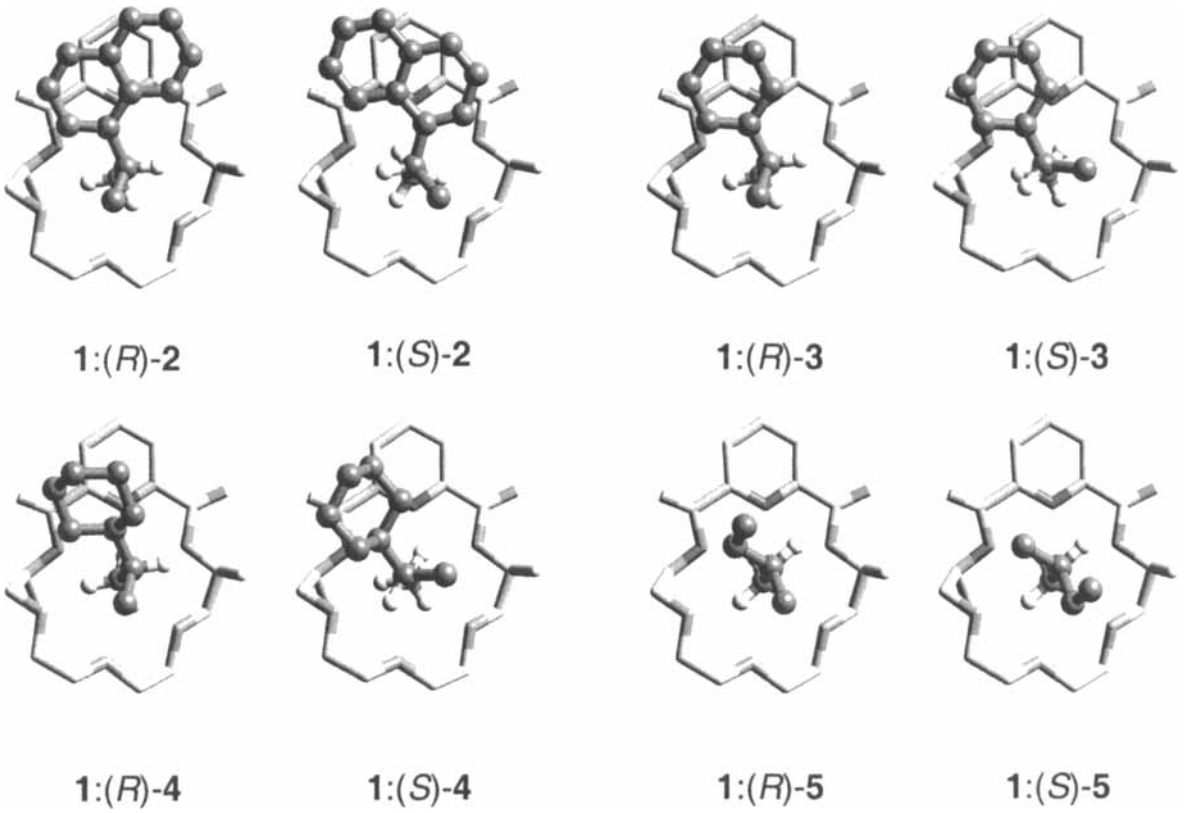

FIGURE 2 Global minimum structures of 1:Guest complexes obtained from high-temperature (800 K) dynamics

for comparing the structures of the two states and to reveal the structural features crucial for the enantioselection. MC/SD runs were performed at 300 K for 10 ns with a 1-fs time step. Samples during the dynamics simulation were obtained every 500 fs. Energy minimization with the conjugate gradient algorithm was then performed on every sampled structure to a gradient norm of less than 0.001 kJ/mol·Å. All the calculations above were performed in vacuo to allow comparison with the experiments in the gas phase.

III. RESULTS AND DISCUSSIONS

FEP Study

In order to obtain a starting geometry conformation, a high-temperature (800 K) MD was used. All conformations of host-guest complexes generated from MD were energy-minimized. The global minimum energy structures obtained in this process are shown in Figure 2. After analyzing the structure of every minimum, we concluded that the crown ring structure of host **1** remains roughly planar in every host-guest complex regardless of the structure and chirality of the guest. Thus we can characterize the structures of host-guest complexes by two angles: As depicted in Figure 3, the tilt angle θ is defined by the atoms C1-N1-N2, and the dihedral angle φ by the atoms C1-C2-N1-N2. Table I lists the values of θ and φ of global minimum structures. The (+) sign is used for counterclockwise rotation of φ while the (–) sign is used for clockwise rotation. The values of θ and φ in the *X*-ray crystal structure of **1**:(*S*)-**2** are 76° and –42°, respectively, and 75° for θ and 42° for φ in **1**:(*R*)-**2**

crystal structure. Even though the values of φ in the calculated structures are different from those in the crystal structures, the energy difference of 3.2 kJ/mol between **1**:(*S*)-**2** and **1**:(*R*)-**2** is comparable to the result of Bradshaw et al.[16] The structures obtained from molecular simulation in the gas phase and *X*-ray crystallography can differ slightly due to the constraints imposed by the crystal packing and the presence of counter-anions in the crystal structure. The pyridine group of **1** and the naphthyl group of **2** (or the phenyl group of **3**) are almost parallel as in the crystal structures, roughly corresponding to the range $70° < \theta < 80°$ in **1:2** and **1:3** complexes.

The FEP-calculated and experimentally determined values for the enantioselectivities of **1** toward **2–5** are given in Table II. The calculated values are in excellent agreement with the experimental results. Only in the case of **1:3** complex the error bar of the experimental value lies outside the standard deviation of the computed result, and even in this case these error intervals are separated by only 0.4 kJ/mol. Moreover, the simulations can reproduce the relative enantioselectivities of **1** toward the guests. **1**:(*R*)-Guest is always more stable than **1**:(*S*)-Guest in every **1**:Guest complex as in the experiments. Figure 4 shows the free energy profiles for the conversion of the (*S*)-Guest into the (*R*)-Guest of each complex. In each case, the free energy profile shows a smooth transition as the (*S*)-Guest mutates into the (*R*)-Guest, and this is consistent with good convergence. To confirm the convergence, we performed a more elaborate FEP calculation with a 100-ps run for equilibration and a 1000-ps run for sampling each window, and the results are listed in Table II. The other conditions are the same as described in part II. The results of this calculation are almost identical to those given by the case of the 100-ps equilibrium and 500-ps sampling simulation. This shows that values of 100 ps for equilibration and 500 ps for sampling per window are adequate for these systems.

The directions of the naphthyl rings of **1**:(*R*)-**2** and **1**:(*S*)-**2** obtained from a high-temperature

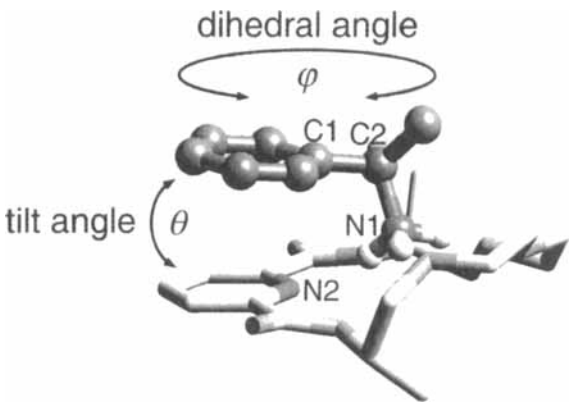

FIGURE 3 The tilt angle (θ) and the dihedral angle (φ) used in describing the host-guest complexes. θ is defined by the atoms C1-N1-N2 and φ by the atoms C1-C2-N1-N2

global minimum search are opposite to those observed in *X*-ray experiments.[19] As a consequence of the difference in orientation of the naphthyl group, different steric interactions between **1**:(*R*)-**2** and **1**:(*S*)-**2** were reported.[32] This is reflected in a shorter contact distance between the methyl carbon attached to the chiral carbon of **1** and the nearest naphthyl hydrogen in (*S*)-**2** than in (*R*)-**2**. To obtain a reliable result, this ring rotation should be included in the phase sampling during the FEP calculation. However, this ring rotation is hardly sampled by traditional molecular dynamics simulations since the energy barrier of the ring rotation is quite high. In our preliminary work,[33] the ring rotation was not properly sampled by traditional molecular dynamics simulations. The torsional energy barriers for the naphthyl ring rotation of (*R* or *S*)-**2** are depicted in Figure 5. In these calculations, the torsional angle connecting the naphthyl group and the chiral carbon was used as the variable, and it is denoted as ω hereafter. When (*R* or *S*)-**2** is not bound to **1**, the energy barrier is about 60 kJ/mol (Figure 5(a)), and when it is bound to **1** the energy barrier is about 90 kJ/mol (Figure 5(b)). To take the ring rotation into account, ω was used as a degree of freedom in Monte Carlo moves in MC/SD. The naphthyl

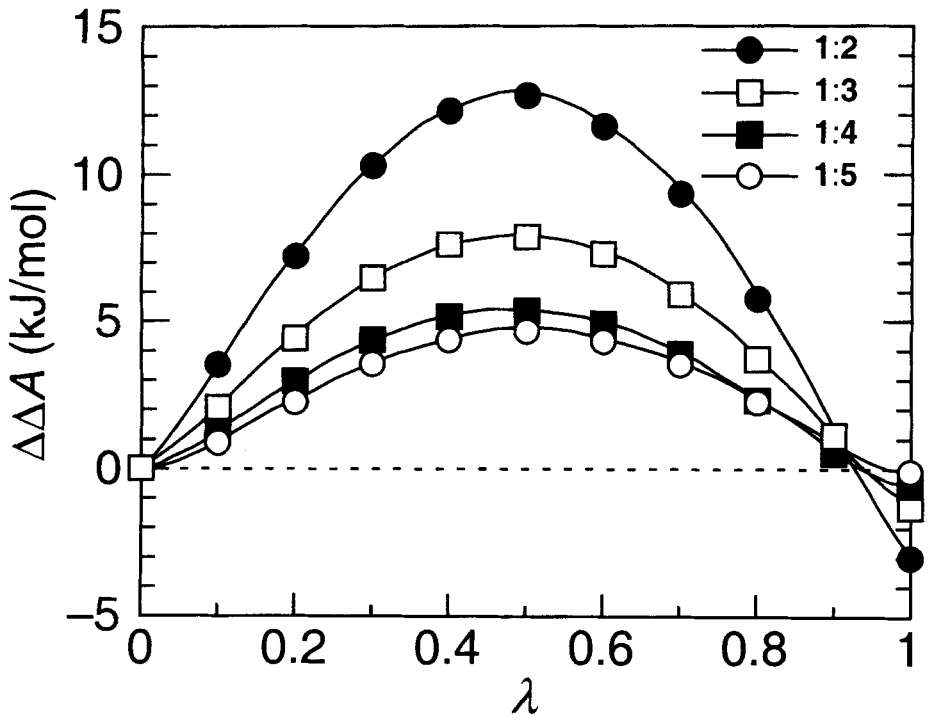

FIGURE 4 Free energy profiles for FEP calculations of **1**:Guest complexes: filled circle **1:2**; open square **1:3**; filled square **1:4**; and open circle **1:5**

ring rotation was observed in the FEP calculation when $\lambda > 0.5$. This shows that the ring rotation motion was properly sampled in our FEP simulation.

MD Simulation

As shown in experimental and FEP results, the degree of enantioselectivity of host **1** toward chiral guests depends on the properties of the largest substituent of the guest. **1** revealed higher enantioselectivity toward the guest with a more rigid and more aromatic substituent. For deeper understanding of the role of the substituent of the guest in enantioselection, MD simulations were performed for every host-guest complex. Even though FEP calculation is suitable for reproducing experimental free energy differences, the structural information of molecules can be obtained more successfully through analysis of the MD trajectories.

The calculated results for $\Delta\Delta A_{Dyn}$ are listed in Table II. Three independent simulations were performed and average values with standard deviations are reported. As in the FEP calculation, the relative enantioselectivities, $\Delta\Delta A_{Dyn}$, were well reproduced. However, the free energy differences obtained in this calculation are less satisfactory than the results of the FEP calculation. According to Figure 5(b), the equilibrium values of ω in **1**:(*R*)-**2** and **1**:(*S*)-**2** are 70° and −90°, repectively. The populations of the Boltzman distribution around these minima at 300 K are about 97% for **1**:(*R*)-**2** and 99% for **1**:(*S*)-**2**, and thus we did not take ω as a variable in the MC/SD simulations.[34] The error from the omission of this degree of freedom is expected to be less than 3%.

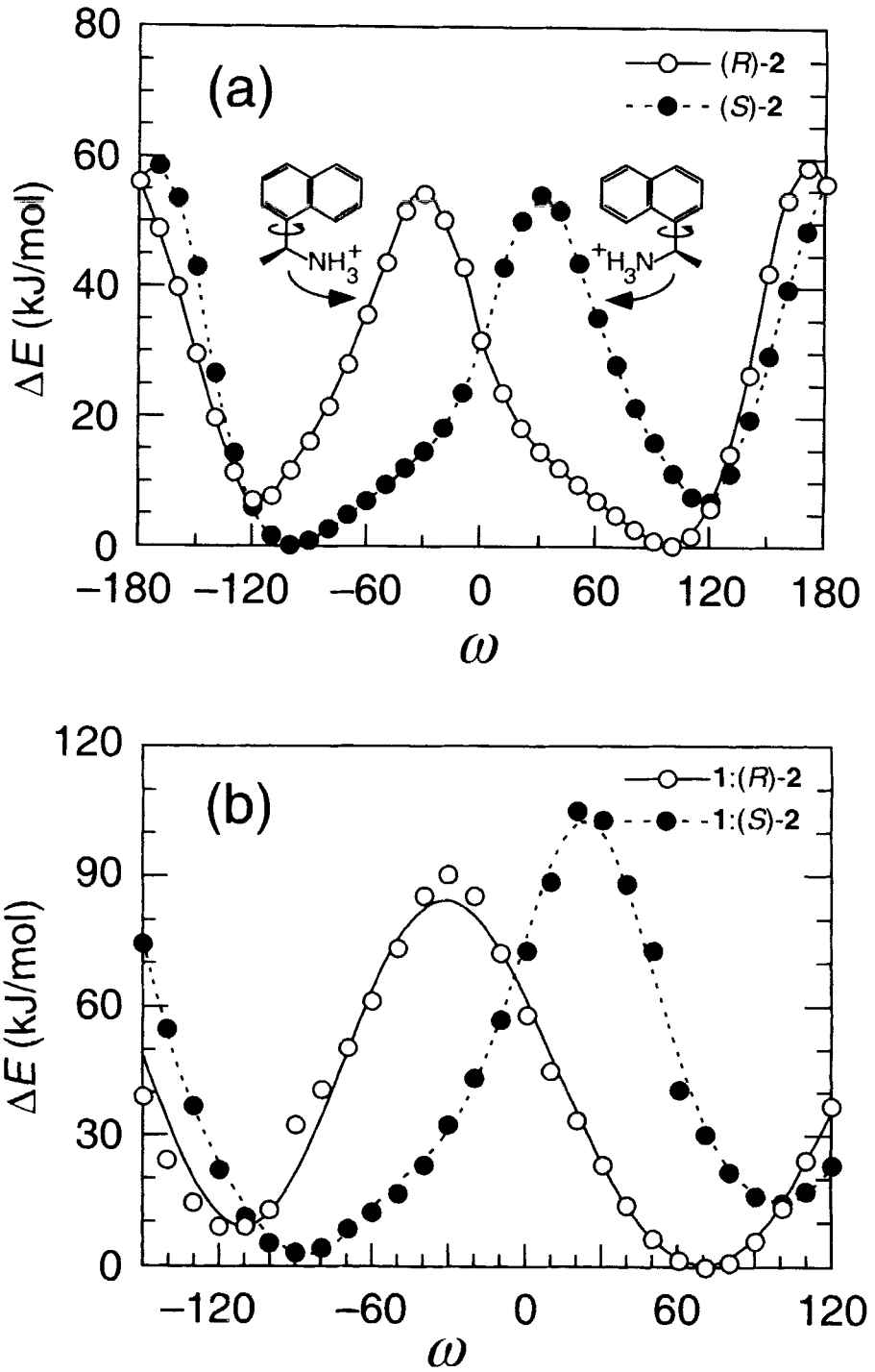

FIGURE 5 Torsional energy profiles for the naphthyl ring rotation of (*R* or *S*)-**2**, (a) when it is not bound to **1** and (b) bound to **1**. ω is the torsional angle connecting the naphthyl group and the chiral carbon. The lines in (b) are the fits to the Fourier series of cosω

TABLE I The Values of φ and θ of Global Minimum Structures of 1:(*R* or *S*)-Guest Complexes Obtained by High Temperature (800 K) Dynamics Simulation

Guest	*(S)*-2	*(R)*-2	*(S)*-	*(R)*-3	*(S)*-4	*(R)*-4	*(S)*-5	*(R)*-5
θ	74°	73°	78°	73°	88°	78°	130°	86°
φ	−14°	35°	30°	38°	38°	43°	−163°	74°

TABLE II Calculated and Experimentally Determined Enantioselectivity of **1** toward **2–5** (All Units are in kJ/mol)

Guest	$\Delta\Delta G_{Exp}$[a]	$\Delta\Delta A_{FEP}$[b]	$\Delta\Delta_{FEP}$[c]	$\Delta\Delta A_{Dyn}$[d]
2	3.5 ± 0.6	3.1 ± 0.3	3.0 ± 0.3	3.8 ± 0.1
3	2.4 ± 0.5	1.3 ± 0.2	1.5 ± 0.1	3.6 ± 0.5
4	0.9 ± 0.2	0.6 ± 0.3	0.5 ± 0.2	3.4 ± 0.9
5	0.3 ± 0.4	0.2 ± 0.2	0.3 ± 0.2	0.8 ± 0.7

a. Experimental values. See Reference 13.
b. Free energy obtained by FEP with 500-ps sampling per window.
c. Free energy obtained by FEP with 1000-ps sampling per window.
d. Free energy obtained by MD.

Although enantioselectivity from MD is less satisfactory than that from FEP, the mechanism of enantioselection can be more clearly elucidated by analysis of the MD trajectories. To analyze the dynamics simulation results more efficiently, we plot the relative occurrence of the configurations on the potential energy surface. The potential energy surface was obtained by the relaxed scan method.[24] The relative angles-θ and φ in Figure 3-between the host and the guest were used as variables in this relaxed scan calculation. We performed energy minimization calculations in the range $50° < \theta < 150°$ and $-180° < \varphi < 180°$. The variation interval was 5° for both θ and φ. The global minima found in this calculation almost coincide with the high-temperature global minimum search results. Only the regions of the potential energy surface with energy up to 20 kJ/mol are presented for clarity, and isoenergy surfaces are represented by contours with an interval of 5 kJ/mol.

The potential energy surfaces of 1:(*R* or *S*)-**2** are shown in Figure 6. As expected from experimental results, most thermally accessible configurations of 1:(*R*)-**2** are located in the range $15° < \varphi < 65°$, while those of 1:(*S*)-**2** are mainly located in the range $-45° < \varphi < 15°$. In both systems, the values of θare around 75°, indicating that the pyridine group of **1** and the naphthyl group of **2** are almost parallel in every local minimum structure. The relative populations found in the MD simulation are also presented in Figure 6 (c)and (d) after analyzing every structure of the MD simulation. As expected from the potential energy surface, structures are located around the region $15° < \varphi < 65°$ for 1:(*R*)-**2**, and in the region $-40° < \varphi < 15°$ for 1:(*S*)-**2**. This result implies that the characterization of host-guest complex structure by θ and φ describes the MD trajectories quite well. As shown in 1:(*S*)-**2** complex, the shape of the θ-φ potential energy surface is almost the same as that from dynamics simulation results. For clarity and efficiency, the θ-φ potential energy surface will be used in the subsequent discussion for elucidating the results of dynamics simulations instead of plotting the structural results in terms of θ and φ.[35]

In order to estimate the contribution of the naphthyl and the methyl groups in **1:2** complex to the enantioselection, potential energy surfaces of 1:Achiral guest were also studied. The achiral guests were constructed by replacing the methyl group attached to the chiral carbon with a hydrogen atom. In these potential energy surfaces, the role of the naphthyl group of **2** in enantiomeric discrimination will be more clearly elucidated. The range and interval of this calculation were the same as above. To understand the role of the direction of the naphthyl ring, we constructed two configurations of 1:Achiral-**2** complexes. One configuration, denoted by $\mathbf{1:2}^{A}_{R}$, was constructed from 1:(*R*)-**2**, and the other, $\mathbf{1:2}^{A}_{S}$, was constructed from 1:(*S*)-**2**, and the structures are shown in Figure 7. These two 1:Achiral-**2** complexes are actually just different conformers of the same complex with a large barrier between them. The structures of these complexes are the same except for the direction

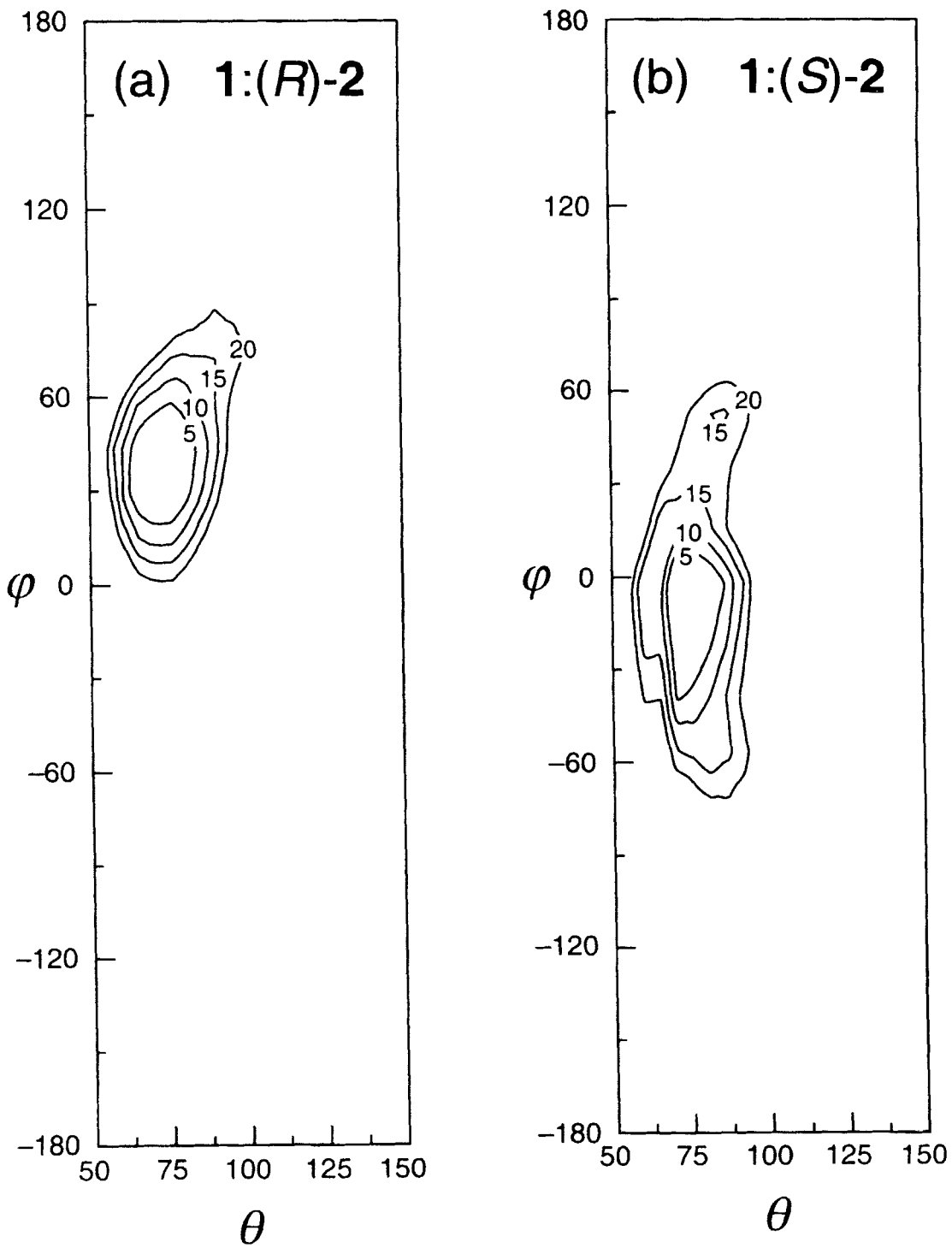

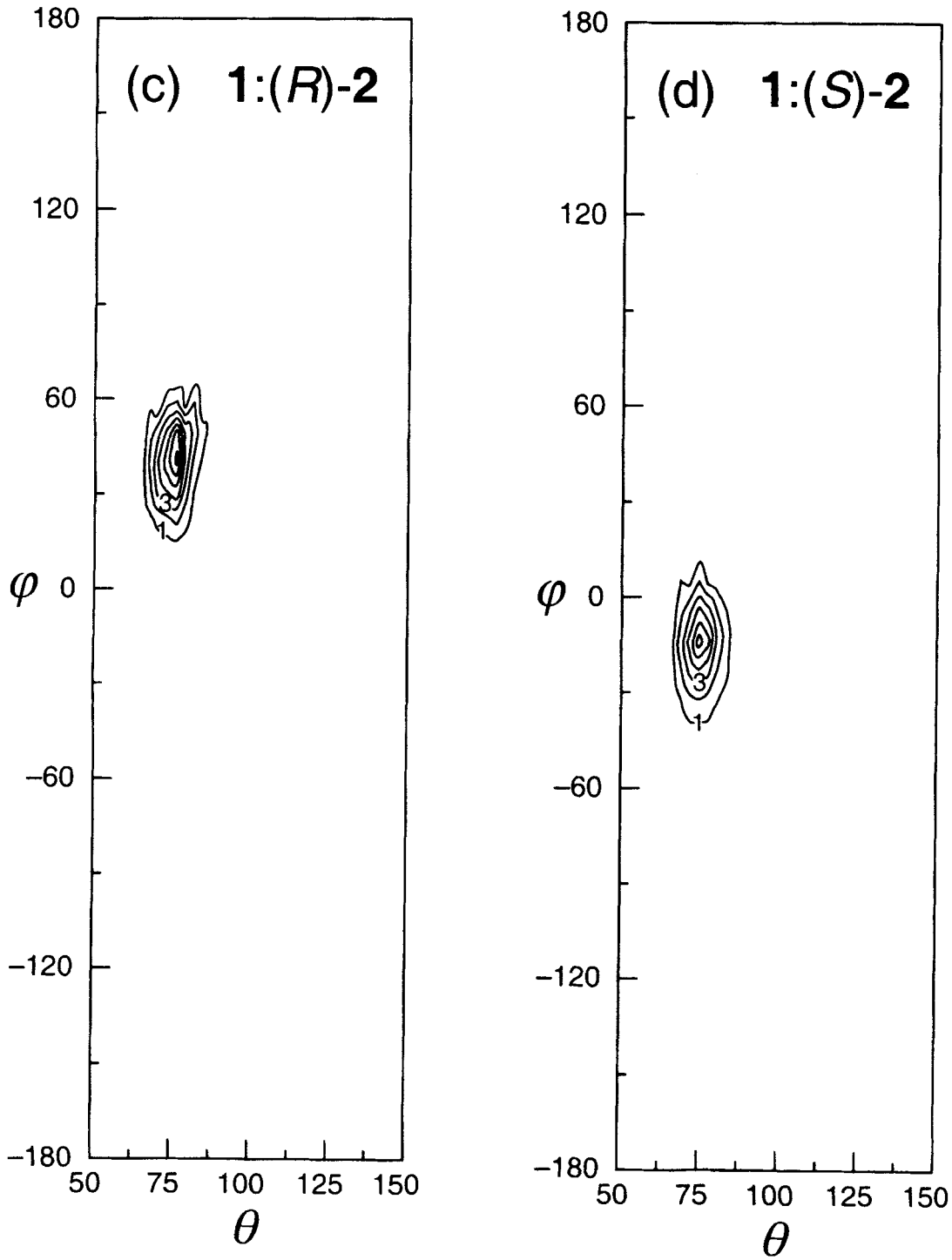

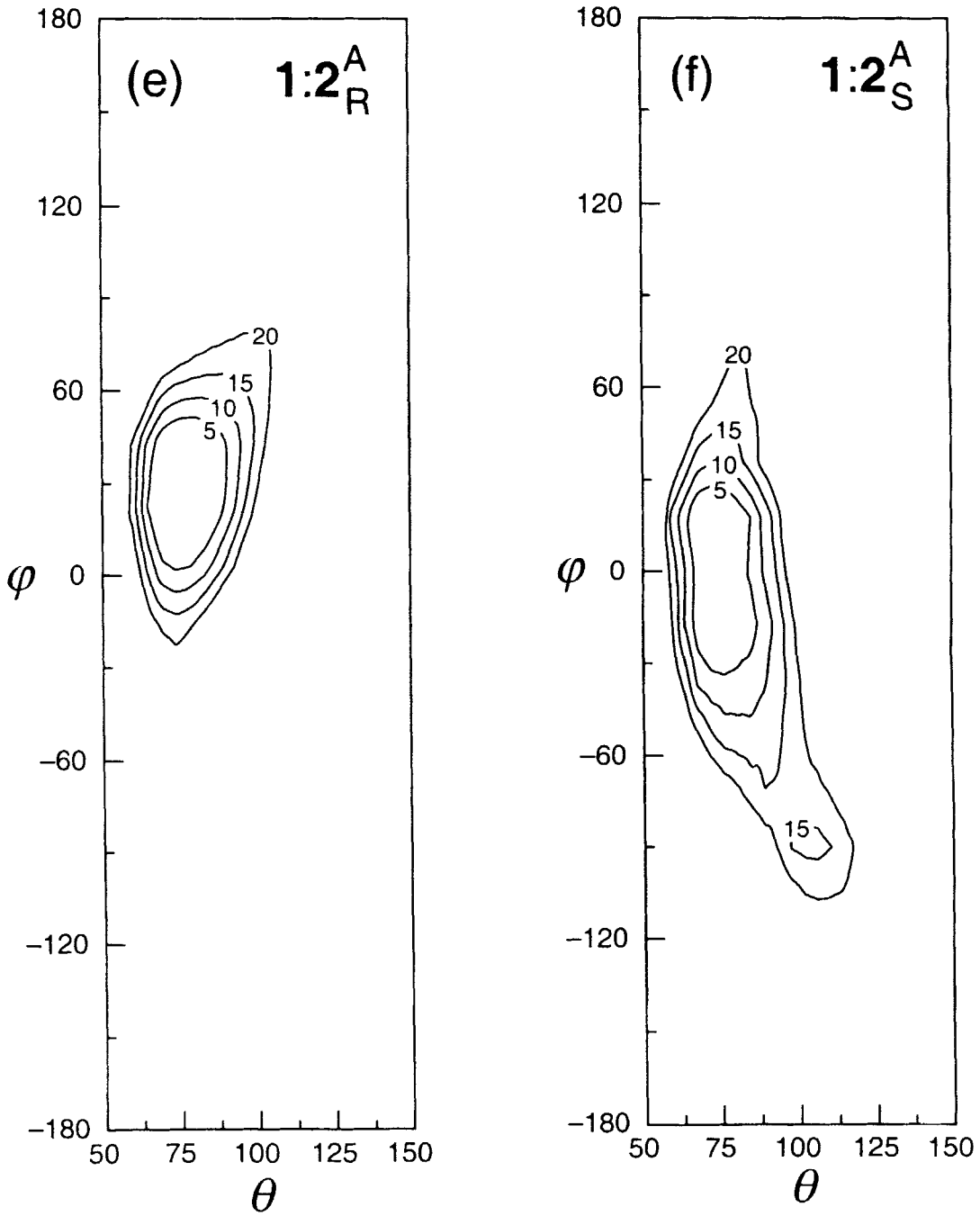

FIGURE 6 (a) and (b): Potential energy surfaces for **1**:(*R*)-**2** and **1**:(*S*)-**2** complexes, respectively. (c) and (d): Relative populations (%) of the conformations in an area element of 5° in θ and φ generated from MD simulations of **1**:(*R*)-**2** and **1**:(*S*)-**2**, respectively. (e) and (f): Potential energy surfaces for $\mathbf{1}:\mathbf{2}^{A}_{R}$, and $\mathbf{1}:\mathbf{2}^{A}_{S}$ complexes, respectively. See Figure 3 for the definition of the angles

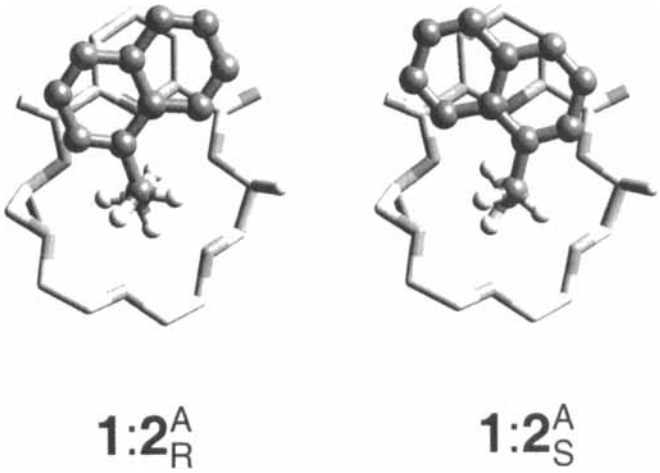

FIGURE 7 The minimum energy structures of (a) $\mathbf{1}:\mathbf{2}^{A}_{R}$ and (b) $\mathbf{1}:\mathbf{2}^{A}_{S}$ complexes

of the naphthyl ring. In principle, an achiral guest cannot be discriminated by a chiral host. Actually, however, in $\mathbf{1}:\mathbf{2}^{A}_{R}$ and $\mathbf{1}:\mathbf{2}^{A}_{S}$ systems, the achiral guests can be discriminated by a chiral host since the directions of the naphthyl rings are opposite. In these complexes, **1** feels these rings differently since the energy barrier for naphthyl ring rotation is as high as 50–60 kJ/mol.

The θ-φ potential energy surfaces of $\mathbf{1}:\mathbf{2}^{A}_{R}$ and $\mathbf{1}:\mathbf{2}^{A}_{S}$ complexes are in Figure 6 (e) and (f). They differ markedly from each other and thermally accessible configurations are mainly located around $-5° < \varphi < 60°$ for $\mathbf{1}:\mathbf{2}^{A}_{R}$ and $-50° < \varphi < 40°$ for $\mathbf{1}:\mathbf{2}^{A}_{S}$. The localized position of $\mathbf{1}:\mathbf{2}^{A}_{R}$(or $\mathbf{1}:\mathbf{2}^{A}_{S}$) is almost the same as that of **1**:(*R*)-**2** (or **1**:(*S*)-**2**). However, the chiral guest is localized to a smaller region on the θ-φ potential energy surfaces. This suggests that the role of the naphthyl ring is to restrict the configuration of the guest relative to the host, even when an achiral guest is docked in a chiral host **1**. When the chiral guest is docked with the host, the methyl group of the guest restricts the complex structure to a more rigid one. This agrees well with the experimental results of Dearden et al., suggesting that the role of the naphthyl ring is more important in enantioselection.

To quantify the role of the naphthyl ring in enantioselection, the MD simulations of $\mathbf{1}:\mathbf{2}^{A}_{R}$ and $\mathbf{1}:\mathbf{2}^{A}_{S}$ were performed and analyzed. The MD conditions were the same as those for the **1**:(*R* or *S*)-**2** complex. The free energy difference in this calculation was 3.6 ± 1.0 kJ/mol. As shown in Figure 6(e) and (f), the potential energy surfaces of $\mathbf{1}:\mathbf{2}^{A}_{R}$ and $\mathbf{1}:\mathbf{2}^{A}_{S}$ are relatively flat and the thermally accessible areas are broader. The error in the free energy difference for the achiral guest is larger than that for the chiral guest. Even though this calculation is relatively rough, it can be concluded that the free energy difference (3.8 ± 0.1 kJ/mol in Table I) in **1:2** mainly comes from the effect of the different ring directions of the naphthyl group.

The θ-φ potential energy surfaces of **1**:(*R* or *S*)-**3**, **1**:(*R* or *S*)-**4**, and **1**:(*R* or *S*)-**5** are shown in Figure 8. As in **1**:(*R* or *S*)-**2**, the location of the global minimum is different between **1**:(*R*)-Guest and **1**:(*S*)-Guest in all complexes, but the difference between them is less than that between **1**:(*R*)-**2** and **1**:(*S*)-**2**. The shapes of the potential energy surfaces of **1**:(*R*)-**5** and **1**:(*S*)-**5**

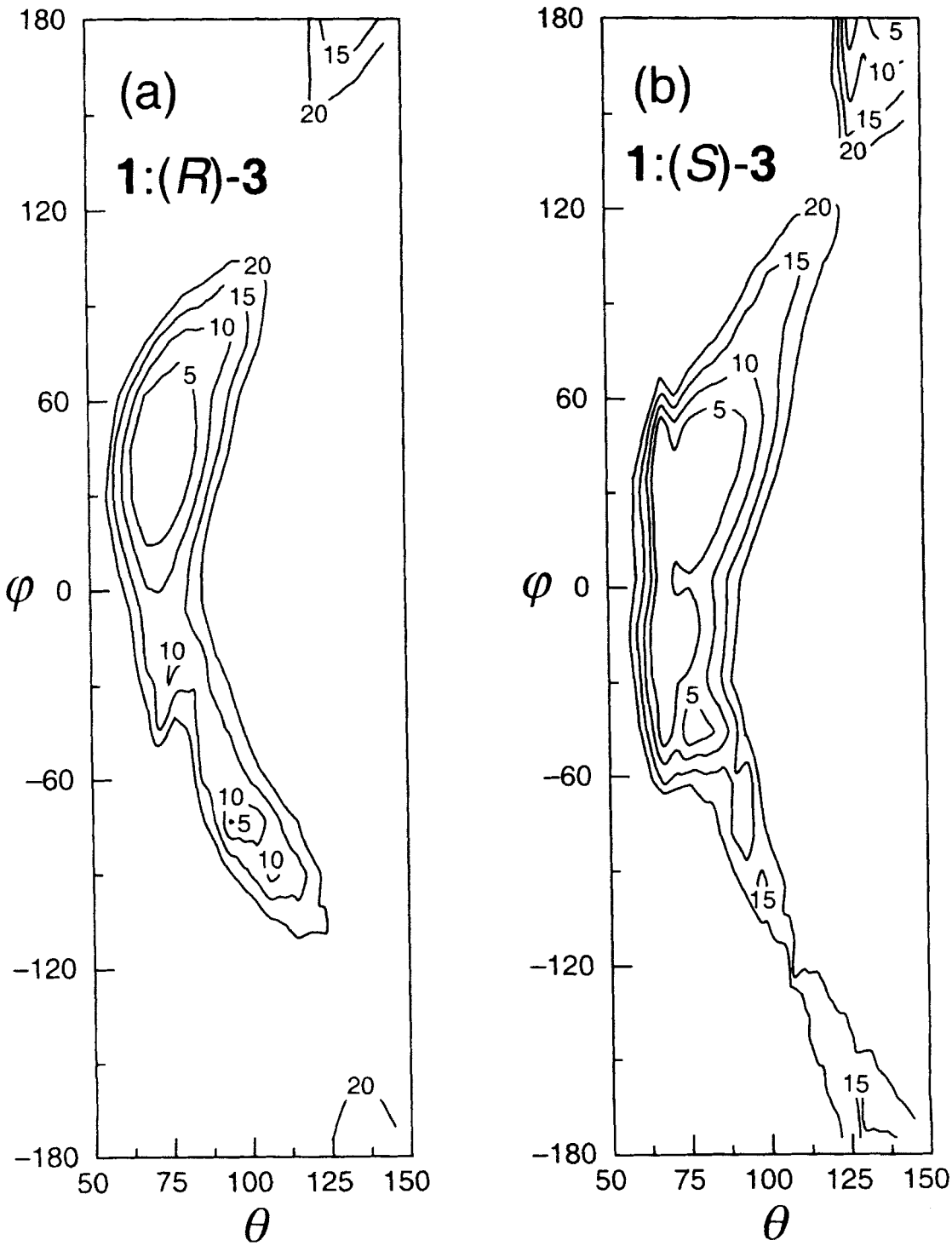

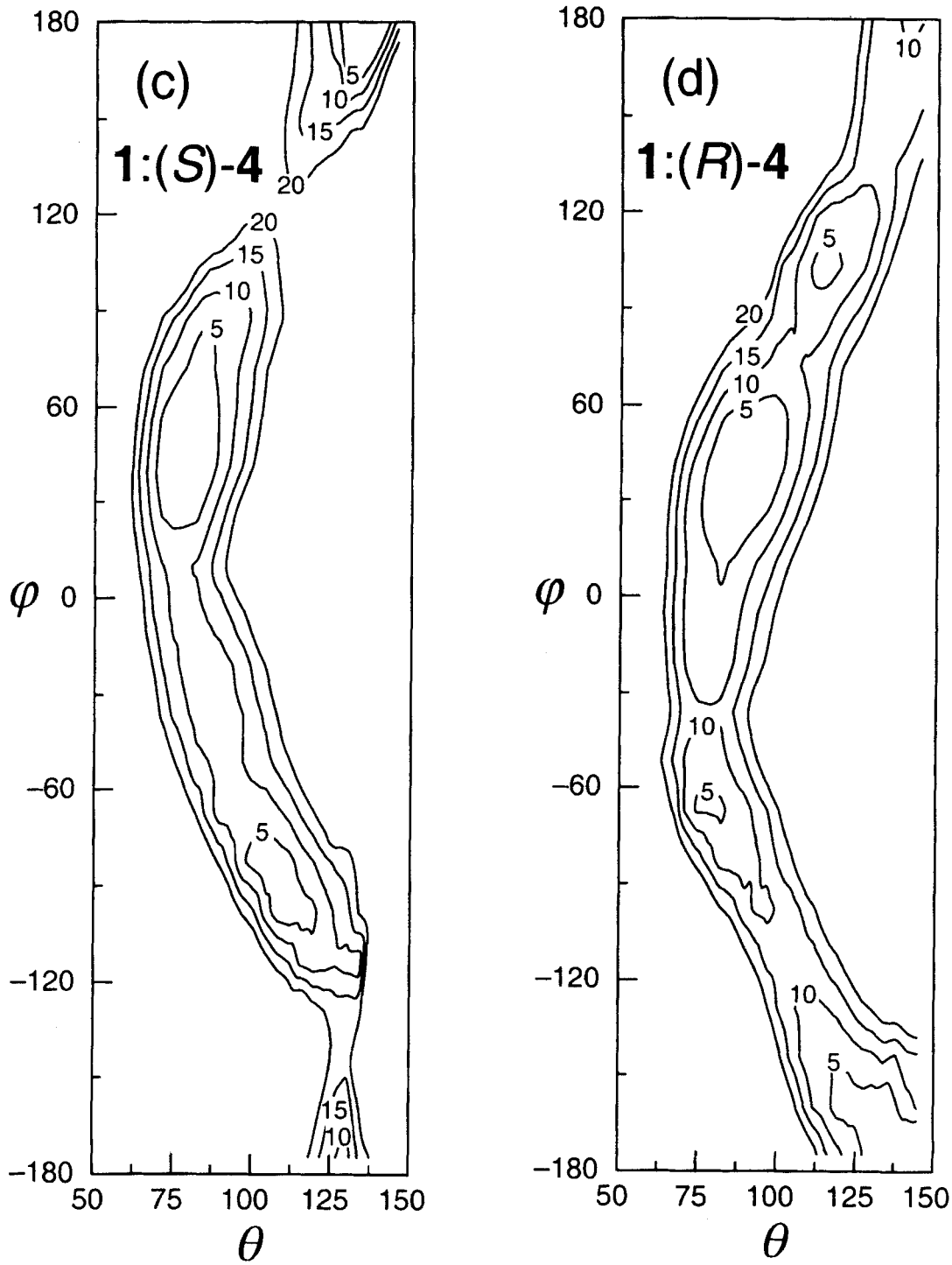

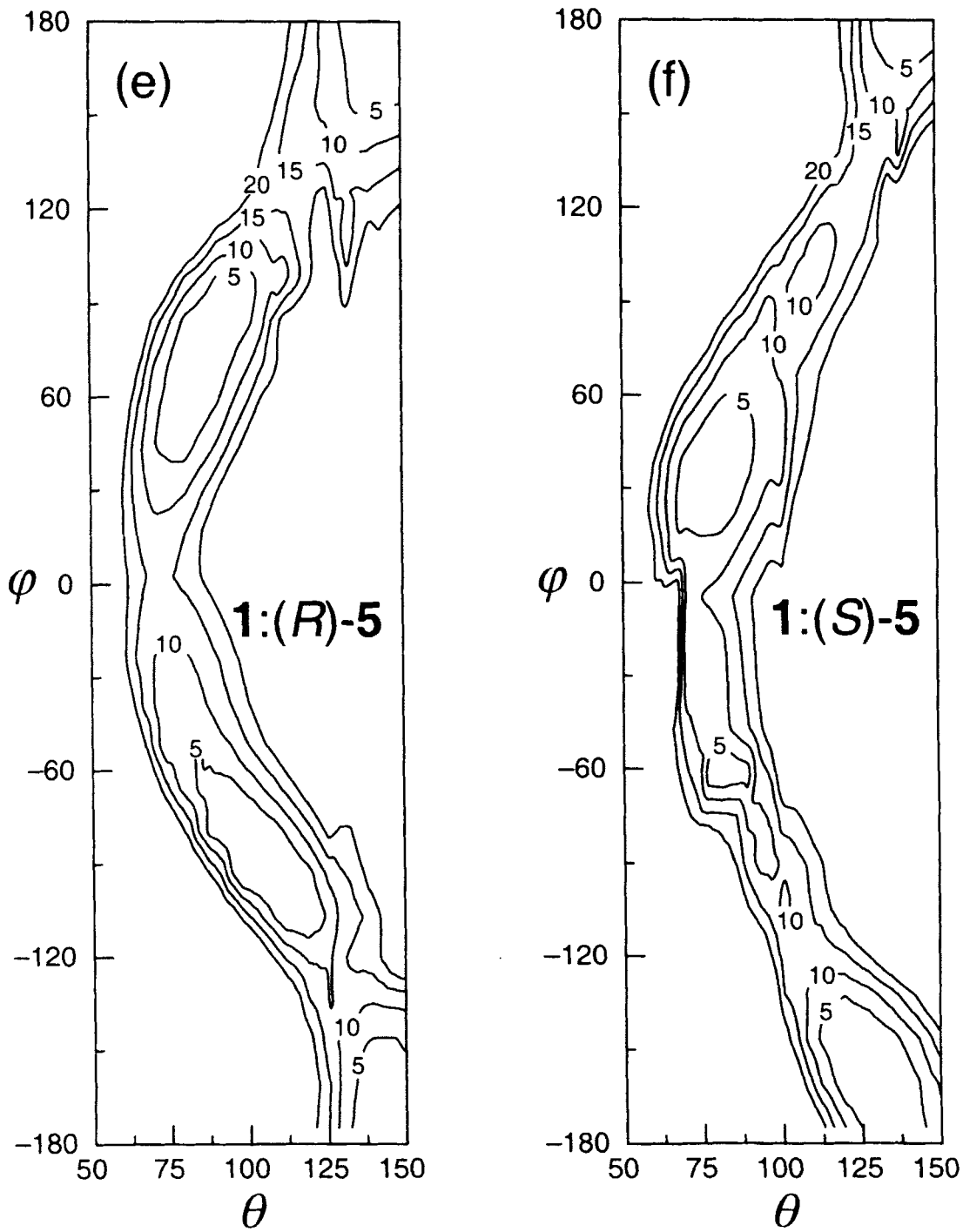

FIGURE 8 Potential energy surfaces for (a) **1**:(*R*)-**3**, (b) **1**:(*S*)-**3**, (c) **1**:(*R*)-**4**, (d) **1**:(*S*)-**4**, (e) **1**:(*R*)-**5**, and (f) **1**:(*S*)-**5** complexes. See Figure 3 for the definition of the angles

are almost the same, and the location of the minima are distributed almost evenly in the range $-180° < \varphi < 180°$, unlike in the other cases. Thus the thermally accessible conformations are spread almost over the full range of the θ-φ potential energy surface. The barriers between them are at most 10 kJ/mol. Moreover, the energy difference between **1**:(*R*)-**5** and **1**:(*S*)-**5**at a corresponding position on the θ-φ potential surface is small. Thus the free energy difference between **1**:(*R*)-**5** and **1**:(*S*)-**5**is small, indicating that host **1** does not discriminate well between (*R*)-**5** and (*S*)-**5**. The θ-φ potential energy surfaces of **1**:(*R* or *S*)-**3** and **1**:(*R* or *S*)-**4** complexes show a relatively moderate tendency toward enantioselection compared with the above two extreme cases, **1**:(*R* or *S*)-**2** and **1**:(*R* or *S*)-**5**. However, in **1**:(*R* or *S*)-**3** complex, the thermally accessible configurations are restricted to a smaller region than in **1**:(*R* or *S*)-**4**, due to the more rigid and the largest aromatic substituent (phenyl group) of **3**.

In summary, we performed FEP and MD simulations on enantiomeric complexes of dimethyldiketopyridino-18-crown-6 (**1**) and chiral protonated amines (**2-5**) to obtain the free energy differences, and to elucidate the mechanism for enantioselectivity. The FEP calculation reproduced the experimental enantioselectivity quite well, and the inclusion of the ring rotation in the FEP simulation was an important factor in reproducing the enantioselectivity in **1:2** complex. In MD simulations, the detailed motion of host-guest complexes was monitored and the role of the substituent of the guest was analyzed. The role of the largest substituent of the guest is to orient the guest to a more stable position relative to the host molecule. When the largest substituent group of the guest is more rigid and more aromatic, the thermally accessible configurations on the θ-φ potential energy surface are restricted to a smaller region, indicating that the more rigid host-guest complex shows a higher enantioselectivity. The methyl group in the guest contributes additional enantioselection by restricting the complex structure to a more rigid one.

Acknowledgements

This work was supported by the Creative Research Initiatives.

References

1) Janoschek, R. *Chirality: From Weak Bosons to the α-Helix*; Springer-Verlag: Berlin, 1991.
2) Thall, E. *J. Chem. Educ.* **1996**, *73*, 481–484.
3) Nielen, M.W.F. *Anal. Chem.* **1993**, *65*, 885–893.
4) Terabe, S.; Shibata, M.; Miyashita, Y. *J. Chromatogr.* **1989**, *480*, 403–411.
5) Kyba, E.P.; Timko, J.M.; Kaplan, L.J.; Jong, F.D.; Gokel, G.W.; Cram, D.J. *J. Am. Chem. Soc.* **1978**, *100*, 4555–4568.
6) Sousa, L.R.; Sogah, G.D.Y.; Hoffman, D.H.; Cram, D.J. *J. Am. Chem. Soc.* **1978**, *100*, 4569–4576.
7) Cram, D.J.; Cram, J.M. *Science* **1974**, *183*, 803–809.
8) Izatt, R.M.; Bradshaw, J.S.; Nielsen, S.A.; Lamd, J.D.; Christensen, J.J.; Sen, D. *Chem. Rev.* **1985**, *85*, 271–339.
9) Inoue, Y.; Gokel, G.W. *Cation Binding by Macrocycles: Complexation of Cationic Species by Crown Ether*; Marcel Dekker, Inc.: New York, 1990.
10) Atwood, J.L. *Inclusion Phenomena and Molecular Recognition*; Plenum Press: New York, 1990.
11) Kuhn, R.; Erni, F.; Bereuter, T.; Häusler, J. *Anal. Chem.* **1992**, *64*, 2815–2820.
12) Zhang, X.X.; Izatt, R.M.; Zhu, C.Y.; Bradshaw, J.S. *Supramol. Chem.* **1996**, *6*, 267–274.
13) Dearden, D.V.; Dejsupa, C.; Liang, Y.; Bradshaw, J.S.; Izatt, R.M. *J. Am. Chem. Soc.* **1997**, *119*, 353–359.
14) Bradshaw, J.S.; Huszthy, P.; Redd, J.T.; Zhang, X.X.; Wang, T.; Hathaway, J.K.; Young, J.; Izatt, R.M. *Pure Appl. Chem.* **1995**, *67*, 691–695.
15) Wang, T.; Bradshaw, J.S.; Huszthy, P.; Izatt, R.M. *Supramol. Chem.* **1996**, *6*, 251–255.
16) Bradshaw, J.S.; Huszthy, P.; McDaniel, C.W.; Zhu, C.Y.; Dalley, N.K.; Izatt, R. M.; Lifson, S. *J. Org. Chem.* **1990**, *55*, 3129–3137.
17) Kollman, P. *Chem. Rev.* **1993**, 93, 2395–2417.
18) Allen, M.P.; Tildesley, D.J. *Computer Simulation of Liquids*; Clarendon Press: Oxford, 1987.
19) Davidson, R.B.; Dalley, N.K.; Izatt, R.M.; Bradshaw, J.S.; Campana, C.F. *Isr. J. Chem.* **1985**, *25*, 33–38.
20) Izatt, R.M.; Zhu, C.Y.; Dalley, N.K.; Curtis, J.C.; Kou, X.; Bradshaw, J.S. *J. Phys. Org. Chem.* **1992**, *5*, 656–662.
21) McCammon, J.A. *Science* **1987**, *238*, 486–491.
22) Armstrong, D.W.; Ward, T.J.; Armstrong, R.D.; Beesley, T.E. *Science* **1986**, *23*, 1132–1135.
23) Pirkle, W.H.; Pochapsky, T.C. *Chem. Rev.* **1989**, *89*, 347–362.
24) Mohamadi, F.; Richards, N.G.J.; Guida, W.C.; Liskamp, R.; Lipton, M.; Caufield, C.; Chang, G.; Hendrickson, T.; Still, W.C. *J. Comput. Chem.* **1990**, *11*, 440–467.
25) Guarnieri, F.; Still, W.C. *J. Comput. Chem.* **1994**, *15*, 1302–1310.
26) Zwanzig, R.W. *J. Chem. Phys.* **1954**, *22*, 1420–1426.
27) Kirkwood, J.G. *J. Chem. Phys.* **1935**, *3*, 300–313.
28) Hwang, S.; Lee, K.H.; Ryu, G.H.; Jang, Y.H.; Lee, S.B.; Lee, W.Y.; Hong, J.-I.; Chung, D.S. *in press (J. Org. Chem.)*.
29) Wang, J.; Kollman, P.A. *J. Am. Chem. Soc.* **1998**, *120*, 11106–11114.

30) Jorgensen, W.L.; Ravimohan, C. *J. Chem. Phys.* **1985**, *83*, 3050–3054.
31) Aerts, J. *J. Comput. Chem.* **1995**, *16*, 914–922.
32) Davidson, R.B.; Bradshaw, J.S.; Jones, B.A.; Dalley, N.K.; Christensen, J.J.; Izatt, R.M.; Morin, F.G.; Grant, D.M. *J. Org. Chem.* **1984**, *49*, 353–357.
33) Lee, O.-S.; Hwang, S.; Chung, D.S. Free Energy Perturbation Study on Enantioselectivity of Crown Ethers. Asianalysis IV, Fukuoka, Japan, May 21–23, 1997; Japan Society for Analytical Chemistry: 1997; 2C10, 70.
34) Lipkowitz, K.B.; Demeter, D.A.; Zegarra, R.; Larter, R.; Darden, T. *J. Am. Chem. Soc.* **1988**, *110*, 3446–3452.
35) Lipkowitz, K.B.; Demeter, D.A.; Parish, C.A.; Darden, T. *Anal. Chem.* **1987**, *59*, 1731–1733.